HHS Public Access

Author manuscript

Biochim Biophys Acta Mol Cell Biol Lipids. Author manuscript; available in PMC 2020 December 01.

Published in final edited form as:

Biochim Biophys Acta Mol Cell Biol Lipids. 2019 December ; 1864(12): 158532. doi:10.1016/j.bbalip.2019.158532.

Endothelial Acid Ceramidase in Exosome-Mediated Release of NLRP3 Inflammasome Products during Hyperglycemia: Evidence from Endothelium-Specific Deletion of *Asah1* Gene

Xinxu Yuan[1], **Owais M. Bhat**[1], **Hannah Lohner**[1], **Yang Zhang**[2], **Pin-Lan Li**[1]

[1]Department of Pharmacology and Toxicology, Virginia Commonwealth University, School of Medicine, Richmond, VA, USA

[2]Department of Pharmacological & Pharmaceutical Sciences, College of Pharmacy, University of Houston, Houston, TX, USA

Abstract

Exosomes have been demonstrated to be one of the mechanisms mediating the release of intracellular signaling molecules to conduct cell-to-cell communication. However, it remains unknown whether and how exosomes mediate the release of NOD-like receptor pyrin domain 3 (NLRP3) inflammasome products such as interleukin-1 beta (IL-1β) from endothelial cells. The present study hypothesized that lysosomal acid ceramidase (AC) determines the fate of multivesicular bodies (MVBs) to control the exosome-mediated release of NLRP3 inflammasome products during hyperglycemia. Using a streptozotocin (STZ)-induced diabetes mouse model, we found that endothelium-specific AC gene knockout mice (*Asah1*$^{fl/fl}$/EC^{cre}) significantly enhanced the formation and activation of NLRP3 inflammasomes in coronary arterial ECs (CECs). These mice also had increased thickening of the coronary arterial wall and reduced expression of tight junction protein compared to wild-type (WT/WT) littermates. We also observed the expression of exosome markers such as CD63 and alkaline phosphatase (ALP) was augmented in STZ-treated *Asah1*$^{fl/fl}$/EC^{cre} mice compared to WT/WT mice, which was accompanied by an increased IL-1β release of exosomes. In the primary cultures of CECs, we demonstrated that AC deficiency markedly enhanced the formation and activation of NLRP3 inflammasomes, but significantly down-regulated tight junction proteins when these cells were exposed to high levels of glucose. The CECs from *Asah1*$^{fl/fl}$/EC^{cre} mice had decreased MVB-lysosome interaction and increased IL-1β–containing exosome release in response to high glucose stimulation. Together, these results suggest that AC importantly controls exosome-mediated release of NLRP3 inflammasome products in CECs, which is enhanced by AC deficiency leading to aggravated arterial inflammatory response during hyperglycemia.

Correspondence sent to: Pin-Lan Li, M.D, Ph.D, Department of Pharmacology & Toxicology, Medical College of Virginia Campus, Virginia Commonwealth University, Richmond, VA 23298, Tel: 804-828-4793, Fax: 804-828-4794, pin-lan.li@vcuhealth.org.

Declaration of competing interest

We declare that there is no conflict of interest to disclose

Keywords

Exosomes; NLRP3 inflammasome; diabetes mellitus; acid ceramidase; lysosome

Introduction

NOD-like receptor pyrin domain 3 (NLRP3) inflammasome activation has been recently known as a novel mechanism of diabetic vascular endothelial dysfunction [1–2]. In response to elevated level of blood glucose, the main NLRP3 inflammasome components including NLRP3, apoptosis-associated speck-like protein (*ASC*) and caspase-1 are aggregated and assembled to form a high molecular weight inflammasome complex within a variety of cells such as endothelial cells (ECs) [3], macrophages[4], renal podocytes[5] and neurons [6], where procaspase-1 is cleaved to its active form, active caspase-1. This active caspase subsequently converts its substrates such as pro-interleukin-1β (IL-1β) to bioactive IL-1β [7–9]. IL-1β release initiates and promotes the inflammatory response causing the consequent pathogenesis of vascular inflammation, atherosclerosis [10–11] and hypertension [12], which may be a crucial mechanism responsible for the development of cardiovascular disease during obesity, metabolic syndrome and diabetes mellitus [13]. Recent studies have demonstrated that the formation and activation of NLRP3 inflammasome indeed occurs in the endothelium of coronary arteries in the early stage of diabetic mice [3]. Although these previous studies confirmed the pathogenic role of NLRP3 inflammasome activation in ECs, it remains poorly understood how this NLRP3 inflammasome activation instigates vascular tissue inflammation. In particular, the NLRP3 inflammasome is formed in the cytoplasm and its products may not be secreted out of cells via the classic protein secretion pathway through Golgi transport and release. It is imperative to study how the inflammasome products such as IL-1β are secreted to trigger the inflammatory responses.

In previous studies in phagocytes, several potential pathways have been assumed to mediate IL-1β release including the exocytosis of IL-1β-containing secretory lysosomes, release of IL-1β from shed plasma membrane microvesicles, fusion of multivesicular bodies with the plasma membrane and subsequent release as IL-1β-containing exosomes, possible specific membrane transporters, and release due to cell lysis [14–15]. To our knowledge, no studies have been done in ECs to elucidate the mechanisms by which inflammasome products are released to trigger vascular inflammation. However, many recent studies have indicated that exosomes are importantly involved in the regulation of endothelial functions [16–17], and exosome-mediated vascular injury may play a crucial role in the development of cardiovascular diseases such as vascular inflammation and atherosclerosis, the hallmarks of diabetic cardiovascular complications [18]. Exosomes are nanosized membrane vesicles released by fusion of an organelle of the endocytic pathway, namely, the multivesicular body (MVB), with the plasma membrane [19]. Recent studies have reported that the MVB-based release of exosomes is finely controlled by lysosome trafficking and associated with the autophagic pathway [20]. This is because mature MVBs can fuse with lysosomes to deliver their contents for degradation via autophagy [21–22]. Indeed, inhibition of lysosome function with different alkaline agents or lysosomal v-ATPase inhibitors such as bafilomycin A or chloroquine, largely increased exosome secretion in different cells such as neurons,

epithelial cells, and vascular cells [23–25]. It seems clear that lysosome function is important for exosome secretion and in contrast lysosome dysfunction may contribute to the abnormality of exosome secretion. Therefore, the regulatory mechanisms of lysosome function may be implicated in the control of exosome secretion. In this regard, lysosomal sphingolipids are viewed as a classical regulator of lysosome function. In particular, ceramide produced via acid sphingomyelinase (ASM) and degraded by acid ceramidase (AC) [26]. Increased ceramide levels in cells including ECs and vascular smooth muscle cells (SMCs) have been reported to alter lysosome function, in particular, which may lead to dysregulation of autophagic flux and exosome secretion [27–30]. Based on these previous findings, we hypothesized that lysosomal AC might critically control lysosome trafficking to multivesicular bodies (MVBs) and thereby determine the fate of these MVBs, which controls exosome release from ECs. Under pathological conditions such as diabetes mellitus, in addition to increased formation and activation of NLRP3 inflammasomes in ECs, exosome secretion and release of inflammasome products may also be increased to instigate the inflammatory response in the arterial wall, ultimately resulting in vascular inflammation and atherogenesis.

In the present study, we first examined whether AC deletion significantly enhances hyperglycemia-induced formation and activation of NLRP3 inflammasomes and increases thickening of the coronary arteries using a diabetic model produced by injection of STZ in endothelium-specific AC knockout mice (*Asah1*$^{fl/fl}$/EC^{cre}). We also observed whether the AC deficiency enhances exosomes secretion in STZ-treated *Asah1*$^{fl/fl}$/EC^{cre} mice, which was accompanied by the increased release of NLRP3 inflammasome product, IL-1β. Then, we used primary cultures of ECs isolated from WT and *Asah1*$^{fl/fl}$/EC^{cre} mice to explore the mechanisms responsible for exosome secretion and lysosome trafficking and interaction with MVBs and to address whether this exosome secreting mechanism mediates the release of NLRP3 inflammasome product, IL-1β. Our results indicate that endothelial AC plays a critical role in the exosome-mediated release of NLRP3 inflammasome products during hyperglycemia, which is associated with its regulatory actions on lysosome trafficking and interaction with MVBs that determine the fate of MVBs and secretion of exosomes.

Materials and Methods

Mice

Asah1 floxed mice (floxed alpha subunit of *Asah1* gene) were gifted by Dr. Erich Gulbins [31]. *Asah1* floxed mice were crossed with Tek-Cre transgenic mice (the Jackson Laboratory, Bar Harbor, ME, USA, B6.CgTg (Tek-cre) 1Ywa/J 008863) to generate endothelium-specific knockout mice (*Asah1*$^{fl/fl}$/EC^{cre}) [32]. To confirm the specific deletion of *Asah1* gene in the endothelium, each batch of *Asah1*$^{fl/fl}$/EC^{cre} mice were crossed with ROSA mice with floxed GFP (the Jackson Laboratory, Bar Harbor, ME, USA, the Jackson Laboratory, Bar Harbor, ME, USA, B6.129-Gt(ROSA)26Sortm1Joe/J 008606) to produce *Asah1*$^{fl/fl}$/EC^{cre}/ROSA mice, which showed green fluorescence in the endothelium indicating endothelium-specific gene deletion. All wild-type (WT/WT) and *Asah1*$^{fl/fl}$/EC^{cre} male and female mice (8-12 weeks old) were used for the present study. They were bred and maintained in an environmentally controlled animal facility center (25°C and 40~50%

humidity) with a 12-hour light/dark cycle. For experiments, WT/WT and *Asah1*$^{fl/fl}$/EC^{cre} mice were randomly divided into four groups and fed a high-fat diet (HFD) or normal diet (ND) for two weeks. HFD groups of mice were intraperitoneally injected with 120 mg/kg of streptozotocin (STZ) citrate buffer (pH 4.5) for four days, then continued HFD or ND for two weeks to generate a diabetic model. The control (Ctrl) mice were injected intraperitoneally with an equal volume of citrate buffer (pH 4.5). Diabets model was confirmed by measuring fasting (8 hours) blood glucose concentration. When mouse protocols were completed, blood was taken for biochemical analysis, and the mouse heart was harvested for histological and immunocytochemical analysis. All procedures were carried out in accordance with the National Institutes of Health guidelines for the care and use of laboratory animals. All animal protocols were approved by the Institutional Animal Care and Use Committee (IACUC) at Virginia Commonwealth University.

Characterization of Asah1$^{fl/fl}$/EC^{cre} Mice and Diabetic Mice

Genotyping of *Asah1*$^{fl/fl}$/EC^{cre} mice were routinely determined by PCR using tail biopsied with the following 3 pairs of primers: 1. 57447 flp: ACAACTGTGTAGGATTCACGCATTCTCC; 57448 flp: TCGATCTATGAAATGTCGCTGTCGG; 2. oIMR1084 GCGGTCTGGCAGTAAAAACTATC, oIMR1085 GTGAAACAGCATTGCTGTCACTT; 3. oIMR7338 CTAGGCCACAGAATTGAAAGATCT, oIMR7339 GTAGGTGGAAATTCTAGCATCATCC. The first pair was combined to detect WT (482 bp) or the flox allele (585 bp). Pair 2 and Pair 3 were combined to detect the Cre allele (100 bp). Immunohistochemistry was used to detect the expression of AC$^{\alpha}$ and ceramide in the ECs from *Asah1*$^{fl/fl}$/EC^{cre} mouse coronary artery. Immunofluorescence was used to detect the colocalization of AC$^{\alpha}$ vs. lamp-1, AC$^{\alpha}$ vs. vWF, ceramide vs. vWF and Cre vs.vWF for characterization of the *Asah1*$^{fl/fl}$/EC^{cre} mice. IVIS and LacZ staining were used to detect the expression of a nuclear-localized green fluorescent protein/beta-galactosidase fusion protein (GFP-NLS-lacZ or GNZ) in *Asah1*$^{fl/fl}$/EC^{cre}/ROSA mice for confirmation of Cre in ECs. Diabetic mice were confirmed by measurement of the increased blood glucose and body weight (BW).

Isolation and culture of endothelial cells (ECs) from mouse coronary artery

Isolation of mouse coronary arterial ECs was carried out and characterized as previously described [33] [34]. Briefly, the heart was excised and put into a petri-dish filled with ice-cold Krebs-Henseleit (KH) solution. The cleaned heart with intact aorta was filled with HBSS using a 25-gauge needle. The opening of the needle was inserted deep into the heart close to the aortic valve. The aorta was tied with the needle as close to the base of the heart as possible. The pump was started with a 20-ml syringe containing warm Hank's Balanced Salt Solution (HBSS) at a rate of 0.1 ml/min, and the heart was then flushed for 15 min. HBSS was replaced with warm enzyme solution (1 mg/ml collagenase type I, 0.5 mg/ml soybean trypsin inhibitor, 3% BSA, and 2% antibiotic-antimycotic), which was flushed through the heart at a rate of 0.1 ml/min. Perfusion fluid was collected at 30-, 60-, and 90-min intervals. At 90 min, the heart was cut with scissors, and the apex was opened to flush out the cells that collected inside the ventricle. The fluid was centrifuged at 1,000 rpm for 10 min, the cell-rich pellets were mixed with one of the media described below, and the cells

were plated in 2% gelatin-coated six-well plates and incubated in 5% CO2-95% O2 at 37°C. The control coronary ECs were cultured in Dulbecco's modified Eagle's medium (DMEM) (Gibco, USA) with 5.5 mM of glucose. For the treatment of cells, ECs were cultured in DMEM with 25 mM of glucose for 24 hours.

Western Blot Analysis

Western blot was used to analyze specific proteins as described previously [35]. Treated ECs were homogenized in RIPA lysis buffer for 30 min on ice. Total protein was measured using Bio-Rad Protein Assay Dye (Bio-rad,500006, USA) and was normalized to 1 μg/ml. 20 μg of protein was loaded into the wells of a 12% SDS-PAGE gel and run for 2-3 hours at a voltage of 100 V. Protein in the gel was transferred to nitrocellulose membranes (Millipore, IPVH00110, USA) at a voltage of 100 V for 1 hour in the cold room. The membrane was blocked in Tris-buffered saline with Tween-20 (TBST) buffer containing 5% non-fat milk (Bio-Rad, 1706404, USA) for 1 hour at room temperature. The blot was incubated with primary antibodies overnight at 4°C. The following antibodies were used for immunoblotting: procaspase-1 (1:1000, Abcam, ab138483, USA) and cleaved-caspase-1 (1:500, Cell Signaling, 67314, USA). The second antibody labeled with HRP was performed for 1 hour at room temperature. The signal was detected using Odyssey FC Imaging. Anti-β-actin antibody (1:20,000 dilution, Santa Cruz, USA) was used to probe this housekeeping gene expression as a loading control. Image J 6.0 (NIH, Bethesda, MD, USA) or Odyssey software was used to quantify the intensity of the specific protein.

Immunofluorescence Staining

Frozen heart sections or CES cultured on cover slides were fixed in 4% paraformaldehyde (PFA) for 10-15 minutes on ice. Samples were permeabilized in 0.1% Triton X-100 for 10 minutes at room temperature and incubated with the following primary antibodies, respectively, for 2 hours or overnight at 4°C: lysosome marker, anti-Lamp-1 antibody (1:500, Abcam, ab25245); exosome marker, anti-CD63 antibody (1:100, Santa Cruz, sc-15363), anti-ALP; MVB marker, anti-VPS16 antibody (1:200, Abcam, ab172654); a prototype of NLRP3 inflammasome product, anti-IL-1β antibody (1:200, BD, AF-401-NA); inflammasome component, anti-NLRP3 (1:200, Abcam, ab4207), *ASC* (1:100, Santa Cruz, sc-22514), and procaspase-1 (1:100, Santa Cruz, sc-56036) antibodies. Then, samples were incubated with a second antibody labeled with either Alexa-488- or Alexa-555 for 1 hour at room temperature in the dark room. Pictures were taken by a confocal laser scanning microscope (Fluoview FV1000; Olympus, Tokyo, Japan). The staining intensity of the cells or tissues was measured and analyzed with Image J 6.0 (NIH, Bethesda, MD, USA). The colocalization between different antibodies was detected with double staining and measured with Image-Pro Plus version 6.0 software (Media Cybernetics, Bethesda, MD). Pearson correlation coefficient (PCC) was used to represent the colocalization of different proteins as described previously [36].

Immunohistochemistry

The paraffin sections from hearts were baked for 30 min at 65°C. Deparaffinization was performed in xylene for 10 minutes, and hydration was carried out in graded ethanol (100%, 95%, 75%) for 5 minutes at room temperature. 10 mM of sodium citrate buffer (pH 6.0) was

used to retrieve the antigen at 98°C for 15 minutes. 3% H_2O_2 in methanol was used to quench the endogenous peroxidase activity. The sections were blocked with 2.5% horse serum for 1 hour at room temperature. Sections were incubated with the following primary antibodies for 2 hours or overnight at 4°C: anti-CD63 (1:200, exosome marker), anti-ALP (1:100, another exosome marker), and anti-IL-1β (1:100, inflammasome product). Sections were incubated with biotinylated secondary antibodies and a streptavidin-peroxidase complex for 20 minutes at room temperature and then sequentially developed with 3,3′-Diaminobenzidine (DAB) solution for 5 minutes. Finally, the sections were counterstained in hematoxylin (Sigma, 51275, USA) for 5 minutes, dehydrated in graded ethanol (75%, 95%, 100%) and mounted with permount medium (Fisher scientific, SP15-100). Negative controls were prepared without the primary antibodies. The area percentage of the positive staining was calculated in Image Pro Plus 6.0 software [37].

Morphologic Examination and Medial Thickening Analysis

HE staining of heart tissue sections was performed to study the morphological changes as described previously [38]. Briefly, the heart was perfused with cold PBS for 10 minutes and 4% cold PFA for another 10 minutes. The heart was collected and immersed in 10% neutral buffered formalin for more than 48 hours. The formalin-fixed heart was embedded in paraffin and then cut into 5-7 μm serial sections for histopathological evaluation. For HE staining, the sections were deparaffinized using dimethylbenzene and rehydrated with 100%, 95% and 75% ethanol to water and then immersed in the hematoxylin and hydrochloride alcohol. As soon as the color turned to blue, the sections were stained with eosin. After that, the sections were rinsed with running water and dehydrated with different grades of ethanol. Finally, the tissue slides were mounted with DPX. Intimal-medium thickening of coronary arteries was examined using Image-Pro Plus 6.0 software (Media Cybernetics Inc, United States).

In Situ Analysis of Caspase-1 Activity

Caspase-1 activity was performed with a similar protocol described previously [39]. FAM-FLICA Caspase-1 Assay Kit (ImmunoChemistry Technologies, LLC, Bloomington, MN, USA) was used to label active caspase-1 enzyme in the frozen sections of coronary arteries in the heart. The sections were fixed in 4% paraformaldehyde (pH 7.4) for 10 min at room temperature and then washed three times in PBS for 5 min and were incubated for 10 min with PBS containing 0.1% Triton X-100. After washing three times for 5 min in PBS, they were incubated with 3% BSA in PBS for 30 min to block nonspecific binding of antibodies and then incubated with the antibody against vWF (1:500; Abcam) overnight at 4°C. After being washed three times in PBS, the sections were co-stained with Alexa-555-labeled anti-sheep secondary antibody and FLICA reagent (1:10) in the kit for 1.5 hours at room temperature. Then, the sections were washed three times with PBS for 10 min each in the darkroom to decant the secondary antibody solution and FLICA reagent. Finally, the samples were mounted with a drop of mounting medium with DAPI and sealed with nail polish for taking images using a confocal laser scanning microscope (Zeiss LSM 710 LSM). Image Pro-Plus version 6.0 software (Media Cybernetics, Bethesda, MD) was used to measure the colocalization of vWF with activated caspase-1(FLICA staining).

Isolation of Exosomes

Exosomes were isolated by differential ultracentrifugation as described previously [28]. Briefly, cell culture medium or serum from mice was collected and centrifuged at 300 g at 4°C for 10 min to remove detached cells or debris. The supernatant was collected and filtered through 0.22 μm filters to remove contaminating apoptotic bodies, microvesicles, and cell debris. Exosomes were obtained by ultracentrifugation of the supernatant at 100,000 x g for 90 min at 4°C (Beckman 70.1 T1 ultracentrifuge rotator). The exosome pellet was washed with PBS, ultra-centrifuged at 100,000 x g and resuspended in 50 μl of ice-cold filtered PBS. Crude exosome-containing pellets are ready for use or stored at −80°C for further use. For NanoSight microparticle analysis, if needed, the samples can be diluted into filtered PBS and then analyzed.

Nanoparticle Tracking Analysis (NTA)

Nanoparticle Tracking Analysis (NTA) was used to analyze exosomes using the light scattering mode of the NanoSight LM10 (NanoSight Ltd., Amesbury, United Kingdom). Samples were diluted in filtered PBS, and 5 frames (30 s each) were captured for each sample with background level 10, camera level 12 and shutter speed 30. Captured exosomes 3D distribution images were analyzed using NTA software (Version 3.2 Build 16). Particles sized between 50-120nm were calculated.

ELISA Analysis of IL-1β secretion

The culture medium or isolated exosomes were collected for IL-1β quantification with an IL-1β ELISA kit according to the manufacturer's instructions and previous studies [40]. In brief, 200 μl of the culture medium or 50 μg of protein from exosomes were added to a microplate strip well and incubated for 2 h at room temperature. Then, the solution was mixed with IL-1β conjugate and incubated for another 2 h at room temperature. Thorough washes were performed between and after the two incubations. 100 μl of substrate solution was applied to generate chemiluminescence. Chemiluminescent absorbance was determined using a microplate reader at λ=450. The IL-1β level was quantified by relating the sample readings to the generated standard curve.

Statistics

Data were shown as means ± SE. Values were analyzed for significant differences between and within multiple groups using ANOVA for repeated measures, followed by Duncan's multiple-range test. Significant differences between the two groups of experiments were examined using the Student's t-test. The statistical analysis was performed with SigmaPlot 12.5 software (Systat *Software, San Jose, CA, USA*). Statistical significance was defined when $P < 0.05$.

Results

Effects of Endothelium-specific Deletion of AC on the Formation and Activation of NLRP3 Inflammasomes in the Coronary Arterial Endothelium of STZ-treated Mice.

We first examined whether *Asah1* gene deletion in the endothelium is involved in hyperglycemia-induced NLRP3 inflammasome formation and activation in the coronary arterial wall of STZ-treated mice. The diabetic mouse model was established by intraperitoneal injection of STZ and HFD treatment. The blood glucose concentration was much higher in both WT/WT and *Asah1*$^{fl/fl}$/EC^{cre} treated with STZ (491.67 ± 83.64 mg/dl and 465.33 ± 35.15 mg/dl) compared to non-STZ treated mice (142.00 ± 9.07 mg/dl, 143.33 ± 13.54 mg/dl). The mouse body weight (BW) also increased in WT/WT or *Asah1*$^{fl/fl}$/EC^{cre} mice treated with STZ and HFD, but there is no significant difference between WT/WT and *Asah1*$^{fl/fl}$/EC^{cre} (S. Fig. 3). These data suggest that endothelial deletion of the *Asah1* gene in *Asah1*$^{fl/fl}$/EC^{cre} mice does not affect mouse BW and STZ-induced hyperglycemia in our experimental setting.

To determine whether *Asah1* gene deletion in *Asah1*$^{fl/fl}$/EC^{cre} mice is involved in hyperglycemia-induced NLRP3 inflammasome formation and activation, we detected the colocalization of NLRP3 (green) vs. caspase-1 (red) and vWF (red) vs. FLICA (green) in the mouse coronary arterial endothelium. The colocalization of NLRP3 vs. caspase-1 and vWF vs. FLICA was increased in the coronary arterial endothelium of WT/WT mice treated with STZ compared to that in WT/WT control mice. This result suggests that hyperglycemia stimulates endothelial NLRP3 inflammasome formation and activation in WT/WT mice. In *Asah1*$^{fl/fl}$/EC^{cre} mice, AC gene deletion alone did not affect the colocalization of NLRP3 vs. caspase-1 and vWF vs. FLICA, whereas STZ-induced increase in the colocalization of NLRP3 vs. caspase-1 and vWF vs. FLICA were enhanced (Fig. 1A–D). Moreover, immunohistochemical analysis also demonstrated that *Asah1* gene deletion enhanced STZ-induced IL-1β production in the coronary arterial endothelium (Fig. 1E–F). These results suggest that *Asah1* gene is involved in NLRP3 inflammasome formation and activation under diabetic conditions, which promotes the release of NLRP3 inflammasome-dependent IL-1β.

Effects of AC Deficiency in ECs on Mouse Coronary Arterial Thickening and Endothelial Tight Junction Disruption in the Coronary Arterial Wall of STZ-treated Mice

NLRP3 inflammasome formation and activation as well as IL-1β release increased neointima formation [41] or medial thickening of mouse coronary arteries [42]. Therefore, we tested the effects of endothelial AC deletion on medial thickening in coronary arteries from an STZ-induced diabetic mouse model. Morphological examination confirmed that STZ injection caused media thickening of the coronary arterial wall in WT/WT mice, which was further enhanced by AC deletion (Fig. 2A and B). This result indicates that AC may normally counteract diabetic coronary arterial pathology.

Decreased expression of tight junction proteins leads to tight junction disruption, which is a marker event for increased endothelial permeability during vascular endothelial dysfunction [43]. As shown in Fig. 2C–F, STZ markedly decreased the expression of tight junction

proteins ZO-1 and ZO-2 in the endothelial layer of coronary arteries from WT/WT mice as displayed by STZ-induced decreases in the colocalization of endothelial marker vWF (green) with ZO-1 and ZO-2 (red). Such STZ-induced down-regulation of ZO-1 and ZO-2 was further enhanced in the coronary arteries of *Asah1*$^{fl/fl}$/EC^{cre} mice indicating that AC deletion further enhances tight junction disruption in the coronary arterial endothelium of STZ-induced diabetic mice.

Effect of Endothelial AC Deletion on Exosome Secretion in the Coronary Arterial Wall of STZ-treated Mice

The previous studies have demonstrated that the interaction of lysosomes with MVBs contributes to exosome secretion, which may participate in the regulation of MVB fate and exosome secretion [44]. Given that AC is mainly detected in the lysosome and its action on lysosome trafficking or function [45–46], we observed the effect of AC deletion on exosome secretion in the coronary arterial wall of STZ-treated mice. Using IHC staining, we detected the expression of exosome markers, ALP and CD63 in the coronary arterial wall, particularly in the intimal area. Under control condition, the expression level of ALP and CD63 in the coronary arterial wall was higher in *Asah1*$^{fl/fl}$/EC^{cre} mice compared to that in WT/WT mice. STZ treatment increased the expression of ALP and CD63 in the coronary arterial wall of WT/WT mice, and this increase was significantly augmented by *Asah1* gene deletion (Fig. 3A–D). These data clearly showed that endothelial AC deficiency increases exosome secretion induced by hyperglycemia. As shown in Fig. 3E and 3F, we also found that endothelial AC deficiency enhanced exosome numbers in the bloodstream, which was enhanced during hyperglycemia. All of these results suggest that AC gene functionality in ECs is crucial for exosome secretion in the mouse coronary arterial wall and even in the control of blood exosome enrichment.

Effects of Endothelial AC Deletion on Exosome Secretion with IL-1β in the Coronary Arterial Endothelium of STZ-treated Mice

Since there are reports that nonclassical IL-1β secretion is dependent on exosome release in murine macrophages [47], we assessed the contribution of exosomes as IL-1β releasing mechanisms in the coronary arterial endothelium of STZ-treated mice. Using confocal microscopy, we first confirmed that AC gene deletion enhanced exosome secretion induced by hyperglycemia in the coronary arterial endothelium of STZ-treated mice, as shown by the increased colocalization of vWF vs. CD63 and vWF vs. ALP (Fig. 4A–D). It was also found that the colocalization of IL-1β vs. CD63 markedly increased in the coronary arterial wall even in WT/WT mice with STZ injection (Fig. 4E–F). Furthermore, we observed that the colocalization of IL-1β vs. CD63 induced by hyperglycemia was also enhanced by AC gene deletion in the coronary arterial endothelium of STZ-injected mice (Fig.4E–F). These data indicate that IL-1β secretion is accompanied by exosome secretion and suggest that AC may indeed participate in the regulation of exosomes, which are an important mechanism mediating the release of NLRP3 inflammasome product, IL-1β.

Effects of AC Deletion on the Formation and Activation of NLRP3 Inflammasomes Induced by High Glucose in the Primary cultures of Coronary Arterial ECs

To further determine the role of AC in exosome secretion of NLRP3 inflammasome products, we used the primary cultures of coronary arterial ECs from WT/WT and *Asah1*$^{fl/fl}$/EC^{cre} mice to examine the effects of AC gene deletion on the formation and activation of NLRP3 inflammasomes and the associated release of exosomes containing their products. Firstly, we found that high glusoce had no effects on AC expression by Western blot analysis in ECs. (S. Fig. 2A–B) . As shown in Fig. 5A and 5C, the colocalization of NLRP3 vs. *ASC* or caspase-1 increased with high glucose stimulation in WT/WT ECs. The colocalization coefficient of NLRP3 vs. *ASC* or caspase-1 was summarized in Fig. 5B and 5D, indicating the aggregation or assembly of these inflammasome molecules. AC gene deletion augmented the increase in NLRP3 inflammasome formation as displayed by increased colocalization of NLRP3 vs. *ASC* or caspase-1 (Fig. 5A–5D). Using Western blot analysis, activated caspase-1 increased with high glucose stimulation, which was enhanced by AC gene deletion (Fig. 5E and 5F). Biochemical analysis of caspase-1 activity (Fig. 5H) and mature IL-1β production in the cell culture medium (Fig. 5G) showed that AC gene deletion increased glucose-induced NLRP3 inflammasome activation.

Effect of AC Deletion on Tight Junction Disruption Induced by High Glucose in the Primary Cultures of Coronary Arterial ECs

Decreased expression of tight junction proteins leads to tight junction disruption, which is a marker for increased endothelial permeability during vascular dysfunction [43]. Here, we examined whether AC deletion alters high glucose-induced endothelial NLRP3 inflammasome activation that contributes to endothelial tight junction disruption in cultured coronary arterial ECs. It was shown that AC deficiency attenuated the expression of the tight junction marker ZO-1 and ZO-2 in ECs during treatment of high glucose (Fig. 6A and 6C). Densitometric histograms showed that tight junctions were significantly disrupted as indicated by a remarkable reduction of relative fluorescence intensity (RFI) across the cell-cell contact.

Effect of AC Deletion on Exosome-mediated Release of NLRP3 Inflammasome Products Induced by High Glucose in the Primary Cultures of Coronary Arterial ECs

To determine the role of AC in the regulation of exosome secretion and associated NLRP3 inflammasome product release from ECs, we first examined the colocalization of multivesicular body (MVB) marker VPS16 with lysosome marker lamp-1 (yellow dots) using immunofluorescence confocal microscopy, which indicates the interaction of MVBs and lysosomes that determines the MVB fate and exosome secretion. It was found that AC gene deletion markedly decreased the colocalization of VPS16 vs. lamp-1 compared with that in WT/WT ECs, which indicates the reduction of lysosome-MBV interaction that may lead to increased exosome secretion. In these ECs with AC gene deletion, glucose further reduced the colocalization of VPS16 vs. lamp-1 (Fig. 7A–7B). Using nanoparticle tracking analysis (NTA), we found that AC gene deletion in ECs significantly augmented the secretion of exosomes (50-150 nm vesicles), in particular, during treatment of high glucose.

Fig. 7C shows representative 3D histograms of microparticles, where those with the size of 50-150 nm were markedly increased. Summarized data are presented in Fig. 7D showing that vesicles detected at a range of 50-150 nm produced from ECs of mice with AC gene deletion were much more than ECs from WT/WT mice. High glucose further increased the production of these vesicles.

Lastly, we aimed to verify that increased vesicles due to AC deficiency or high glucose are mainly exosomes and such enhanced exosome secretion can mediate the release of IL-1β. To this end, we examined colocalization of exosome marker CD63 and IL-1β around ECs as well as measured IL-1β concentration in purified exosomes. As shown in Fig. 7E–F, there was a significant increase in the colocalization of CD63 with IL-1β in and around ECs treated with high glucose, and such increase was further augumented by AC gene deletion. These results demonstrated a remarkable enhancement of high glucose-induced exosome-driven IL-1β increase in ECs when AC is deficient. Consistently, IL-1β levels from exosomes prepared from EC culture supernatants were significantly increased upon high glucose stimulation, which was further elevated in exosomes from ECs with AC gene deletion (Fig. 7G). Howerver, AC inducer, genistein substantially inhibited exosome release and attenuated its release induced by high glucose in cultured ECs (S. Fig. 4A–B). Genistein also decreased NLRP3 inflammasome formation and activation as shown by reduced colocalization of NLRP3 with ASC or Caspase-1 and IL-1 β production (S. Fig. 4C–G).

Discussion

In the present study, we demonstrated that AC regulates the exosome-mediated release of NLRP3 inflammasome product, IL-1β during hyperglycemia. Our results first proved that AC gene deletion significantly enhanced hyperglycemia-induced formation and activation of the NLRP3 inflammasome leading to IL-1β production in ECs *in vitro* and *in vivo*, which was accompanied by the enhanced exosome-mediated release of this inflammasome product resulting in the inflammatory response in the arterial wall. This inflammation due to NLRP3 inflammasome activation and exosome-mediated release of inflammation activating factors is the triggering mechanism mediating enhanced medial thickening of coronary arteries and EC permeability increase during hyperglycemia. The findings of the present study indicate that AC-mediated signaling plays an important role in the inflammatory response during hyperglycemia via exosome-mediated regulation of NLRP3 inflammasomes.

In previous studies, acid sphingomyelinase and ceramide associated membrane raft signaling platforms have been shown to contribute to endothelial NLRP3 inflammasome activation and arterial neointima formation during hypercholesterolemia [48]. We have also demonstrated that hyperglycemia induces NLRP3 inflammasome activation in the coronary arterial endothelium of STZ-treated mice [3]. However, it remains unknown whether ceramide-mediated signaling is involved in the development of diabetic vasculopathy and how ceramide signaling is involved in NLRP3 inflammasome activation. In particular, it is imperative to investigate how the products of NLRP3 inflammasome activation in the cytoplasm are secreted out of ECs to trigger the inflammatory response in the arterial wall. The present study hypothesized that AC as a metabolizing enzyme of ceramide might

control lysosome trafficking to MVBs regulating the fate of MVBs and consequent secretion of exosomes. AC deficiency may reduce the interaction of lysosome and MVBs leading to exosome secretion, and during hyperglycemia, this increased exosome excretion may mediate the release of products derived from NRLP3 inflammasome activation given that inflammasome products are produced in the cytoplasm and may not be secreted through classic Golgi-mediated direction and transport. To test this hypothesis, we generated endothelium-specific AC gene knockout mice (Asah1$^{fl/fl}$/EC^{cre}) and used these mice and their WT littermates to produce a diabetic model. It is known that endothelial dysfunction at the early stage of cardiovascular diseased is a foundamental mechanism responsible for the development diabetic vasculopathy. Our previous study had already demonstrated that the ROS-dependent activation of endothelial NLRP3 inflammasomes by hyperglycemia was an important initiating mechanism to cause endothelial dysfunction in STZ-induced diabetic mice [3]. Streptozotocin (STZ) have been extensively used in animal models to study both the pathology of diabetes mellitus and complications related to the disease as well as possible interventions [49]. There are many reports that HFD with low doses of STZ could generate a type II diabetes model in mice [50–52] and in rats [53–55]. In our preliminary experiments, we injected mice on the HFD 5 times in total at low-doses of STZ (~60 mg/kg), but it could not generate a stable mouse diabetes model, which may be due to species differences. Then, we increased the dose to 120 mg/kg for 4 days, which led to a stable and typical type 2 diabetes. The dose of STZ was similar to previous reports [52]. Using this animal model, we examined whether NLRP3 inflammasome activation is enhanced and whether NLRP3 inflammasome products can be increasingly released from ECs in mice with deletion of the AC gene in the endothelium. It was found that deficiency of the *Asah1* gene enhanced the formation and activation of NLRP3 inflammasomes in the coronary endothelium of *Asah1*$^{fl/fl}$/EC^{cre} mice and isolated CECs. These results suggest that AC plays an important role in the formation and activation of NLRP3 inflammasomes in coronary arterial endothelial cells which may be a triggering mechanism for diabetic inflammation in the arterial wall. We indeed found that activated coronary endothelia inflammasome in *Asah1*$^{fl/fl}$/EC^{cre} mice was accompanied by increased thickening of the coronary arterial wall and enhanced down-regulation of ZO-1 and ZO-2 in the coronary arterial endothelium compared to their WT littermates similarly treated with STZ. Although we did not test how AC deficiency may induce endothelial inflammasome activation and enhanced endothelial junction dysfunction, previous studies have shown that the deficiency in AC may lead to sphingolipid and phospholipid imbalance, which resulted in chronic lung injury caused by significant inflammation and increased vascular permeability [56]. Loss of AC activity in a murine model of Farber disease was also reported to lead to an early and profound immune-phenotype that reflects alterations in both the innate and adaptive immune cell populations, suggesting that increased levels of ceramide may serve as an important mechanism to activate inflammasome and local inflammatory response upon different pathologic stimuli [57].

One of the most important findings in the present study is that the deficiency of AC in *Asah1*$^{fl/fl}$/EC^{cre} diabetic mice significantly enhanced the expression of exosome markers such as CD63 and ALP in the coronary arterial wall, indicating enhanced secretion of exosomes under such pathological conditions. In isolated CECs, we detected increased

exosome release when *Asah1* gene was deleted. Also, it was found that this increased exosome release was associated with reduced interaction of lysosomes and MVBs which led to reduced degradation of MVBs and thereby resulted in increased exosome release. Moreover, the present study demonstrated that enhanced exosome secretion from CECs from *Asah1*$^{fl/fl}$/EC^{cre} mice carried inflammasome products such as IL-1β, suggesting that AC-dependent exosome release is a crucial mechanism for the secretion of NLRP3 inflammasome products upon hyperglycemia. To our knowledge, these findings for the first time demonstrate that AC critically controls the inflammatory exosome secretion and the activation of local inflammatory responses in the arterial wall during diabetes. Extracellular ATP stimulation was shown to stimulate a P2X7R-induced formation of IL-1β-containing MVBs in murine macrophages, which can be exocytosed via intraluminal vesicles (ILVs) from MVBs [58]. In human THP-1 monocytes and microglia cells, extracellular vesicles including exosomes are also shown to mediate the secretion of IL-1β [59–60]. However, some other studies in activated human monocytes revealed that both pro-IL-1β and caspase-1 are entrapped in these vesicles, which as an endolysosomal compartment undergoes exocytosis in the form of secretory lysosomes [61–62], but not via exosomes. The Atg5-dependent export pathway in the autophagic process was also reported to contribute to the secretion of the pro-inflammatory cytokine IL-1β in different mammalian cells [63]. It seems that different types of cells under various conditions may use distinct mechanisms to release inflammasome products including IL-1β. However, whether the exosome-mediated release of inflammasome products is specific to CECs, but not to other types of cells, remains to be further studied.

In our study, *Asah1* floxed mice were crossed with Tek-Cre (or Tie2-Cre) transgenic mice (the Jackson Laboratory, Bar Harbor, ME, USA, B6.CgTg (Tek-cre) 1Ywa/J 008863) to generate endothelium-specific knockout mice (*Asah1*$^{fl/fl}$/EC^{cre}). Although Tunica intima endothelial kinase 2 (Tie2-Cre) transgenic mice was reported to be a new genetic tool for the analyses of endothelial cell-lineage and endothelial cell-specific gene targeting [32], it has to be noted that Tie2 is also expressed in hematopoietic cells [64]. Therefore, the possibility that the lack of AC in monocytes in the coronary artery may also affect the inflammatory response in coronary artery and thereby participate in the development of coronary artery injury. However, our in vitro cell studies to some extent confirmed that monocytes may not be essential contributor to the activation of endothelial inflammasome and increases in exosome secretion.

In summary, the present study demonstrated that AC deficiency not only enhanced NLRP3 inflammasome activation but also increased the release of inflammasome products such as IL-1β via exosomes secretion in CECs. Both events led to local inflammatory responses resulting in arterial wall inflammation during the development of diabetic vascular complications. Targeting exosome-mediated release of NLRP3 inflammasome products regulated by AC may represent a novel strategy for prevention and treatment of diabetic vasculopathy.

Supplementary Material

Refer to Web version on PubMed Central for supplementary material.

Acknowledgment:

This study was supported by grants (HL122937, HL122769, HL057244, and HL075316) from the National Institutes of Health (NIH).

References:

[1]. Zhang J, Xia L, Zhang F, Zhu D, Xin C, Wang H, Zhang F, Guo X, Lee Y, Zhang L, Wang S, Guo X, Huang C, Gao F, Liu Y, Tao L, A novel mechanism of diabetic vascular endothelial dysfunction: Hypoadiponectinemia-induced NLRP3 inflammasome activation, Biochim Biophys Acta Mol Basis Dis, 1863 (2017)1556–1567. [PubMed: 28216285]

[2]. Chen Z, Martin M, Li Z, Shyy JY, Endothelial dysfunction: the role of sterol regulatory element-binding protein-induced NOD-like receptor family pyrin domain-containing protein 3 inflammasome in atherosclerosis, Curr Opin Lipidol, 25 (2014) 339–349. [PubMed: 25188917]

[3]. Chen Y, Wang L, Pitzer AL, Li X, Li PL, Zhang Y, Contribution of redox-dependent activation of endothelial Nlrp3 inflammasomes to hyperglycemia-induced endothelial dysfunction, J Mol Med (Berl), 94 (2016) 1335–1347. [PubMed: 27783111]

[4]. Zhang X, Dai J, Li L, Chen H, Chai Y, NLRP3 Inflammasome Expression and Signaling in Human Diabetic Wounds and in High Glucose Induced Macrophages, J Diabetes Res, 2017 (2017) 5281358. [PubMed: 28164132]

[5]. Yu Q, Zhang M, Qian L, Wen D, Wu G, Luteolin attenuates high glucose-induced podocyte injury via suppressing NLRP3 inflammasome pathway, Life Sci, 225 (2019) 1–7. [PubMed: 30935950]

[6]. Ward R, Ergul A, Relationship of endothelin-1 and NLRP3 inflammasome activation in HT22 hippocampal cells in diabetes, Life Sci, 159 (2016) 97–103. [PubMed: 26883974]

[7]. dos Santos G, Rogel MR, Baker MA, Troken JR, Urich D, Morales-Nebreda L, Sennello JA, Kutuzov MA, Sitikov A, Davis JM, Lam AP, Cheresh P, Kamp D, Shumaker DK, Budinger GR, Ridge KM, Vimentin regulates activation of the NLRP3 inflammasome, Nat Commun, 6 (2015) 6574. [PubMed: 25762200]

[8]. Strowig T, Henao-Mejia J, Elinav E, Flavell R, Inflammasomes in health and disease, Nature, 481 (2012) 278–286. [PubMed: 22258606]

[9]. Latz E, Xiao TS, Stutz A, Activation and regulation of the inflammasomes, Nat Rev Immunol, 13 (2013) 397–411. [PubMed: 23702978]

[10]. Yin Y, Pastrana JL, Li X, Huang X, Mallilankaraman K, Choi ET, Madesh M, Wang H, Yang XF, Inflammasomes: sensors of metabolic stresses for vascular inflammation, Front Biosci (Landmark Ed), 18 (2013) 638–649. [PubMed: 23276949]

[11]. Duewell P, Kono H, Rayner KJ, Sirois CM, Vladimer G, Bauernfeind FG, Abela GS, Franchi L, Nunez G, Schnurr M, Espevik T, Lien E, Fitzgerald KA, Rock KL, Moore KJ, Wright SD, Hornung V, Latz E, NLRP3 inflammasomes are required for atherogenesis and activated by cholesterol crystals, Nature, 464 (2010) 1357–1361. [PubMed: 20428172]

[12]. Pasqua T, Pagliaro P, Rocca C, Angelone T, Penna C, Role of NLRP-3 Inflammasome in Hypertension: a Potential Therapeutic Target, Curr Pharm Biotechnol, (2018).

[13]. Luo B, Li B, Wang W, Liu X, Xia Y, Zhang C, Zhang M, Zhang Y, An F, NLRP3 gene silencing ameliorates diabetic cardiomyopathy in a type 2 diabetes rat model, PLoS One, 9 (2014) e104771. [PubMed: 25136835]

[14]. Eder C, Mechanisms of interleukin-1 beta release, Immunobiology, 214 (2009) 543–553. [PubMed: 19250700]

[15]. Lopez-Castejon G, Brough D, Understanding the mechanism of IL-1beta secretion, Cytokine Growth Factor Rev, 22 (2011) 189–195. [PubMed: 22019906]

[16]. Davidson SM, Riquelme JA, Zheng Y, Vicencio JM, Lavandero S, Yellon DM, Endothelial cells release cardioprotective exosomes that may contribute to ischaemic preconditioning, Sci Rep, 8 (2018) 15885. [PubMed: 30367147]

[17]. van Balkom BW, de Jong OG, Smits M, Brummelman J, den Ouden K, de Bree PM, van Eijndhoven MA, Pegtel DM, Stoorvogel W, Wurdinger T, Verhaar MC, Endothelial cells require

miR-214 to secrete exosomes that suppress senescence and induce angiogenesis in human and mouse endothelial cells, Blood, 121 (2013) 3997–4006, S3991–3915. [PubMed: 23532734]

[18]. Motawi TK, Shehata NI, ElNokeety MM, El-Emady YF, Potential serum biomarkers for early detection of diabetic nephropathy, Diabetes Res Clin Pract, 136 (2018) 150–158. [PubMed: 29253627]

[19]. Hessvik NP, Llorente A, Current knowledge on exosome biogenesis and release, Cellular and molecular life sciences : CMLS, 75 (2018) 193–208. [PubMed: 28733901]

[20]. Baixauli F, Lopez-Otin C, Mittelbrunn M, Exosomes and autophagy: coordinated mechanisms for the maintenance of cellular fitness, Front Immunol, 5 (2014) 403. [PubMed: 25191326]

[21]. Colombo M, Raposo G, Thery C, Biogenesis, secretion, and intercellular interactions of exosomes and other extracellular vesicles, Annu Rev Cell Dev Biol, 30 (2014) 255–289. [PubMed: 25288114]

[22]. Huotari J, Helenius A, Endosome maturation, EMBO J, 30 (2011) 3481–3500. [PubMed: 21878991]

[23]. Akyurek LM, Yang ZY, Aoki K, San H, Nabel GJ, Parmacek MS, Nabel EG, SM22alpha promoter targets gene expression to vascular smooth muscle cells in vitro and in vivo, Mol Med, 6 (2000) 983–991. [PubMed: 11147575]

[24]. Piccoli E, Nadai M, Caretta CM, Bergonzini V, Del Vecchio C, Ha HR, Bigler L, Dal Zoppo D, Faggin E, Pettenazzo A, Orlando R, Salata C, Calistri A, Palu G, Baritussio A, Amiodarone impairs trafficking through late endosomes inducing a Niemann-Pick C-like phenotype, Biochemical pharmacology, 82 (2011) 1234–1249. [PubMed: 21878321]

[25]. Price PA, Buckley JR, Williamson MK, The amino bisphosphonate ibandronate prevents vitamin D toxicity and inhibits vitamin D-induced calcification of arteries, cartilage, lungs and kidneys in rats, The Journal of nutrition, 131 (2001) 2910–2915. [PubMed: 11694617]

[26]. Gatt S, Enzymic Hydrolysis and Synthesis of Ceramides, J Biol Chem, 238 (1963) 3131–3133. [PubMed: 14081938]

[27]. Serban KA, Rezania S, Petrusca DN, Poirier C, Cao D, Justice MJ, Patel M, Tsvetkova I, Kamocki K, Mikosz A, Schweitzer KS, Jacobson S, Cardoso A, Carlesso N, Hubbard WC, Kechris K, Dragnea B, Berdyshev EV, McClintock J, Petrache I, Structural and functional characterization of endothelial microparticles released by cigarette smoke, Sci Rep, 6 (2016) 31596. [PubMed: 27530098]

[28]. Kapustin AN, Chatrou ML, Drozdov I, Zheng Y, Davidson SM, Soong D, Furmanik M, Sanchis P, De Rosales RT, Alvarez-Hernandez D, Shroff R, Yin X, Muller K, Skepper JN, Mayr M, Reutelingsperger CP, Chester A, Bertazzo S, Schurgers LJ, Shanahan CM, Vascular smooth muscle cell calcification is mediated by regulated exosome secretion, Circulation research, 116 (2015) 1312–1323. [PubMed: 25711438]

[29]. Zhang Y, Xu M, Xia M, Li X, Boini KM, Wang M, Gulbins E, Ratz PH, Li PL, Defective autophagosome trafficking contributes to impaired autophagic flux in coronary arterial myocytes lacking CD38 gene, Cardiovasc Res, 102 (2014) 68–78. [PubMed: 24445604]

[30]. Xu M, Zhang Q, Li PL, Nguyen T, Li X, Zhang Y, Regulation of dynein-mediated autophagosomes trafficking by ASM in CASMCs, Front Biosci (Landmark Ed), 21 (2016) 696–706. [PubMed: 26709800]

[31]. Beckmann N, Kadow S, Schumacher F, Gothert JR, Kesper S, Draeger A, Schulz-Schaeffer WJ, Wang J, Becker JU, Kramer M, Kuhn C, Kleuser B, Becker KA, Gulbins E, Carpinteiro A, Pathological manifestations of Farber disease in a new mouse model, Biol Chem, (2018).

[32]. Kisanuki YY, Hammer RE, Miyazaki J, Williams SC, Richardson JA, Yanagisawa M, Tie2-Cre transgenic mice: a new model for endothelial cell-lineage analysis in vivo, Dev Biol, 230 (2001) 230–242. [PubMed: 11161575]

[33]. Li X, Han WQ, Boini KM, Xia M, Zhang Y, Li PL, TRAIL death receptor 4 signaling via lysosome fusion and membrane raft clustering in coronary arterial endothelial cells: evidence from ASM knockout mice, J Mol Med (Berl), 91 (2013) 25–36. [PubMed: 23108456]

[34]. Kobayashi M, Inoue K, Warabi E, Minami T, Kodama T, A simple method of isolating mouse aortic endothelial cells, J Atheroscler Thromb, 12 (2005) 138–142. [PubMed: 16020913]

[35]. Mo D, Zeng G, Yuan X, Chen M, Hu L, Li H, Wang H, Xu P, Lai C, Wan J, Zhang C, Cheng M, Molecular docking simulation on the interactions of laccase from Trametes versicolor with nonylphenol and octylphenol isomers, Bioprocess Biosyst Eng, 41 (2018) 331–343. [PubMed: 29185034]

[36]. Chen Y, He X, Yuan X, Hong J, Bhat O, Li G, Li PL, Guo J, NLRP3 Inflammasome Formation and Activation in Nonalcoholic Steatohepatitis: Therapeutic Target for Antimetabolic Syndrome Remedy FTZ, Oxidative medicine and cellular longevity, 2018 (2018) 2901871. [PubMed: 30140364]

[37]. Xia M, Boini KM, Abais JM, Xu M, Zhang Y, Li PL, Endothelial NLRP3 inflammasome activation and enhanced neointima formation in mice by adipokine visfatin, Am J Pathol, 184 (2014) 1617–1628. [PubMed: 24631027]

[38]. Chen Y, Li X, Boini KM, Pitzer AL, Gulbins E, Zhang Y, Li PL, Endothelial Nlrp3 inflammasome activation associated with lysosomal destabilization during coronary arteritis, Biochim Biophys Acta, 1853 (2015) 396–408. [PubMed: 25450976]

[39]. Boini KM, Xia M, Abais JM, Li G, Pitzer AL, Gehr TW, Zhang Y, Li PL, Activation of inflammasomes in podocyte injury of mice on the high fat diet: Effects of ASC gene deletion and silencing, Biochim Biophys Acta, 1843 (2014) 836–845. [PubMed: 24508291]

[40]. Li X, Zhang Y, Xia M, Gulbins E, Boini KM, Li PL, Activation of Nlrp3 inflammasomes enhances macrophage lipid-deposition and migration: implication of a novel role of inflammasome in atherogenesis, Plos One, 9 (2014) e87552. [PubMed: 24475307]

[41]. Xia M, Boini KM, Abais JM, Xu M, Zhang Y, Li PL, Endothelial NLRP3 inflammasome activation and enhanced neointima formation in mice by adipokine visfatin, Am J Pathol, 184 (2014) 1617–1628. [PubMed: 24631027]

[42]. Yuan X, Bhat O, Meng N, Lohner H, Li PL, Protective Role of Autophagy in Nlrp3 Inflammasome Activation and Medial Thickening of Mouse Coronary Arteries, Am J Pathol, (2018).

[43]. Bazzoni G, Dejana E, Endothelial cell-to-cell junctions: molecular organization and role in vascular homeostasis, Physiol Rev, 84 (2004) 869–901. [PubMed: 15269339]

[44]. Eitan E, Suire C, Zhang S, Mattson MP, Impact of lysosome status on extracellular vesicle content and release, Ageing Res Rev, 32 (2016) 65–74. [PubMed: 27238186]

[45]. Park JH, Schuchman EH, Acid ceramidase and human disease, Biochim Biophys Acta, 1758 (2006) 2133–2138. [PubMed: 17064658]

[46]. Laurier-Laurin ME, De Montigny A, Attiori Essis S, Cyr M, Massicotte G, Blockade of lysosomal acid ceramidase induces GluN2B-dependent Tau phosphorylation in rat hippocampal slices, Neural Plast, 2014 (2014)196812. [PubMed: 25276436]

[47]. Qu Y, Franchi L, Nunez G, Dubyak GR, Nonclassical IL-1 beta secretion stimulated by P2X7 receptors is dependent on inflammasome activation and correlated with exosome release in murine macrophages, J Immunol, 179 (2007) 1913–1925. [PubMed: 17641058]

[48]. Koka S, Xia M, Chen Y, Bhat OM, Yuan X, Boini KM, Li PL, Endothelial NLRP3 inflammasome activation and arterial neointima formation associated with acid sphingomyelinase during hypercholesterolemia, Redox Biol, 13 (2017) 336–344. [PubMed: 28633109]

[49]. Deeds MC, Anderson JM, Armstrong AS, Gastineau DA, Hiddinga HJ, Jahangir A, Eberhardt NL, Kudva YC, Single dose streptozotocin-induced diabetes: considerations for study design in islet transplantation models, Lab Anim, 45 (2011) 131–140. [PubMed: 21478271]

[50]. Yu T, Sungelo MJ, Goldberg IJ, Wang H, Eckel RH, Streptozotocin-Treated High Fat Fed Mice: A New Type 2 Diabetes Model Used to Study Canagliflozin-Induced Alterations in Lipids and Lipoproteins, Horm Metab Res, 49 (2017) 400–406. [PubMed: 28395380]

[51]. Fan M, Jiang H, Zhang Y, Ma Y, Li L, Wu J, Liraglutide Enhances Autophagy and Promotes Pancreatic beta Cell Proliferation to Ameliorate Type 2 Diabetes in High-Fat-Fed and Streptozotocin-Treated Mice, Med Sci Monit, 24 (2018) 2310–2316. [PubMed: 29664069]

[52]. Obrosov A, Shevalye H, Coppey LJ, Yorek MA, Effect of tempol on peripheral neuropathy in diet-induced obese and high-fat fed/low-dose streptozotocin-treated C57Bl6/J mice, Free Radic Res, 51 (2017) 360–367. [PubMed: 28376643]

[53]. Srinivasan K, Viswanad B, Asrat L, Kaul CL, Ramarao P, Combination of high-fat diet-fed and low-dose streptozotocin-treated rat: a model for type 2 diabetes and pharmacological screening, Pharmacol Res, 52 (2005) 313–320. [PubMed: 15979893]

[54]. Zhang M, Lv XY, Li J, Xu ZG, Chen L, The characterization of high-fat diet and multiple low-dose streptozotocin induced type 2 diabetes rat model, Exp Diabetes Res, 2008 (2008) 704045. [PubMed: 19132099]

[55]. Reed MJ, Meszaros K, Entes LJ, Claypool MD, Pinkett JG, Gadbois TM, Reaven GM, A new rat model of type 2 diabetes: the fat-fed, streptozotocin-treated rat, Metabolism, 49 (2000) 1390–1394. [PubMed: 11092499]

[56]. Yu FPS, Islam D, Sikora J, Dworski S, Gurka J, Lopez-Vasquez L, Liu M, Kuebler WM, Levade T, Zhang H, Medin JA, Chronic lung injury and impaired pulmonary function in a mouse model of acid ceramidase deficiency, Am J Physiol Lung Cell Mol Physiol, 314 (2018) L406–L420. [PubMed: 29167126]

[57]. He X, Schuchman EH, Ceramide and Ischemia/Reperfusion Injury, J Lipids, 2018 (2018) 3646725. [PubMed: 29610685]

[58]. Qu Y, Franchi L, Nunez G, Dubyak GR, Nonclassical IL-1 beta secretion stimulated by P2X7 receptors is dependent on inflammasome activation and correlated with exosome release in murine macrophages, Journal of Immunology, 179 (2007) 1913–1925.

[59]. MacKenzie A, Wilson HL, Kiss-Toth E, Dower SK, North RA, Surprenant A, Rapid secretion of interleukin-1 beta by microvesicle shedding, Immunity, 15 (2001) 825–835. [PubMed: 11728343]

[60]. Bianco F, Pravettoni E, Colombo A, Schenk U, Moller T, Matteoli M, Verderio C, Astrocyte-derived ATP induces vesicle shedding and IL-1 beta release from microglia, Journal of Immunology, 174 (2005) 7268–7277.

[61]. Andrei C, Dazzi C, Lotti L, Torrisi MR, Chimini G, Rubartelli A, The secretory route of the leaderless protein interleukin 1beta involves exocytosis of endolysosome-related vesicles, Molecular biology of the cell, 10 (1999) 1463–1475. [PubMed: 10233156]

[62]. Andrei C, Margiocco P, Poggi A, Lotti LV, Torrisi MR, Rubartelli A, Phospholipases C and A2 control lysosome-mediated IL-1 beta secretion: Implications for inflammatory processes, Proceedings of the National Academy of Sciences of the United States of America, 101 (2004) 9745–9750. [PubMed: 15192144]

[63]. Dupont N, Jiang S, Pilli M, Ornatowski W, Bhattacharya D, Deretic V, Autophagy-based unconventional secretory pathway for extracellular delivery of IL-1beta, Embo J, 30 (2011) 4701–4711. [PubMed: 22068051]

[64]. Tang Y, Harrington A, Yang X, Friesel RE, Liaw L, The contribution of the Tie2+ lineage to primitive and definitive hematopoietic cells, Genesis, 48 (2010) 563–567. [PubMed: 20645309]

Highlights

- Endothelial acid ceramidase regulates hyperglycemia-induced NLRP3 inflammasome activation
- Endothelial exosome release mediates the secretion of NLRP3 inflammasome products
- Lysosomal acid ceramidase finely controls endothelial exosome release

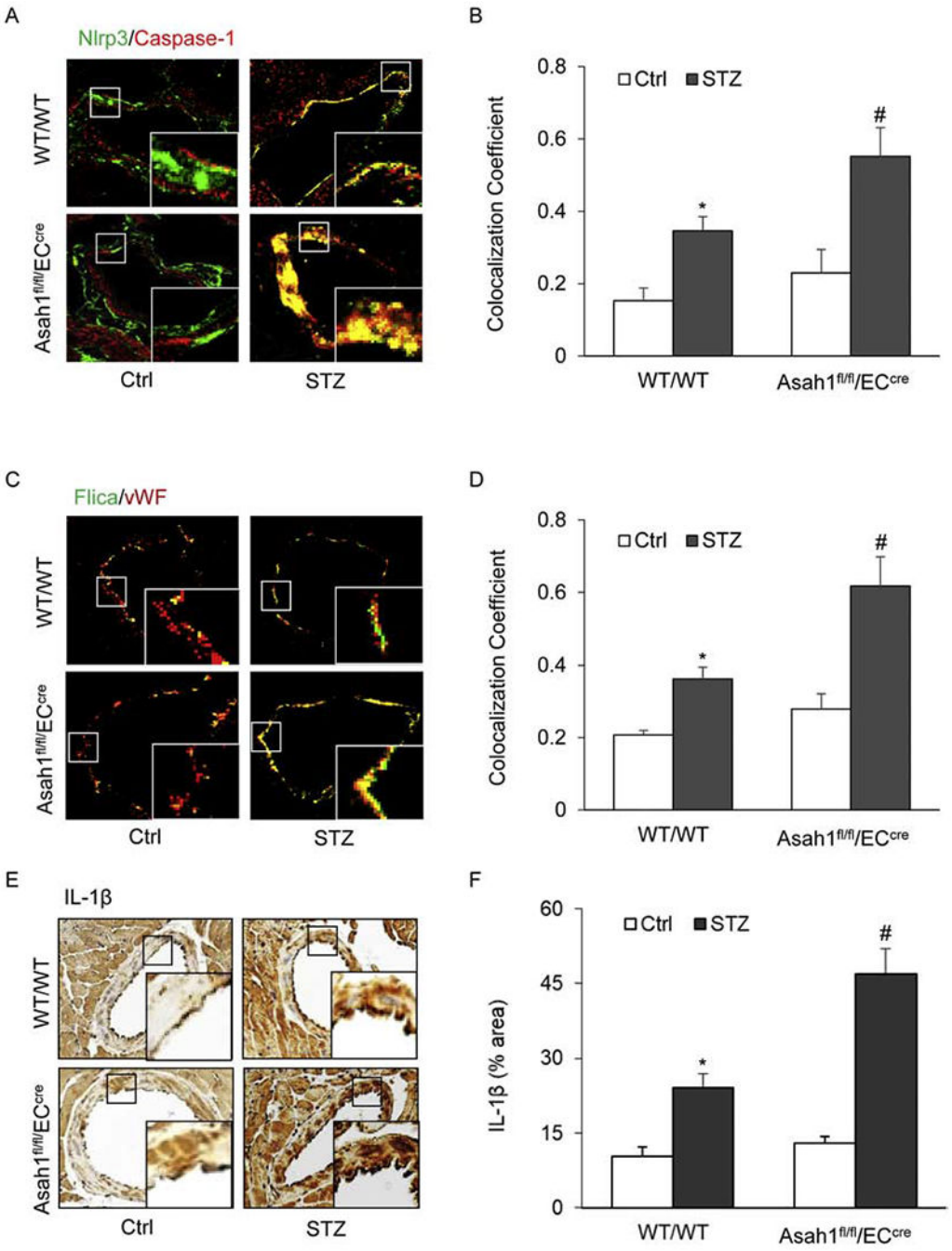

Fig. 1. AC deficiency increased the formation and activation of NLRP3 inflammasomes in the coronary arterial endothelium of STZ-treated mice.

Wild type (WT/WT) and *Asah1* endothelial specific knock-out mice (*Asah1*$^{fl/fl}$/EC^{cre}) were treated with vehicle (Ctrl) or streptozotocin (STZ) as described. A. Representative fluorescent confocal microscopic images displaying the yellow dots or patches showing the colocalization of NLRP3 (green) with caspase-1 (Red). B. The summarized data showing the colocalization coefficient of NLRP3 with caspase-1. C. Representative fluorescent confocal microscopic images displaying the yellow dots or patches showing the colocalization of a green fluorescent probe specific for active caspase-1, FLIC A (green) with vWF (Red), an

endothelium marker. D. The summarized data showing the colocalization coefficient of FLIC A with vWF. E. Representative immunohistochemical staining showing IL-1β accumulation in the coronary arterial wall. F. The summarized data showing the density of IL-1β stained with selective anti-IL-1β antibody. Data are expressed as means ± SEM, n=5. * $p<0.05$ vs. WT/WT-Ctrl group; # $p<0.05$ vs. WT/WT-STZ.

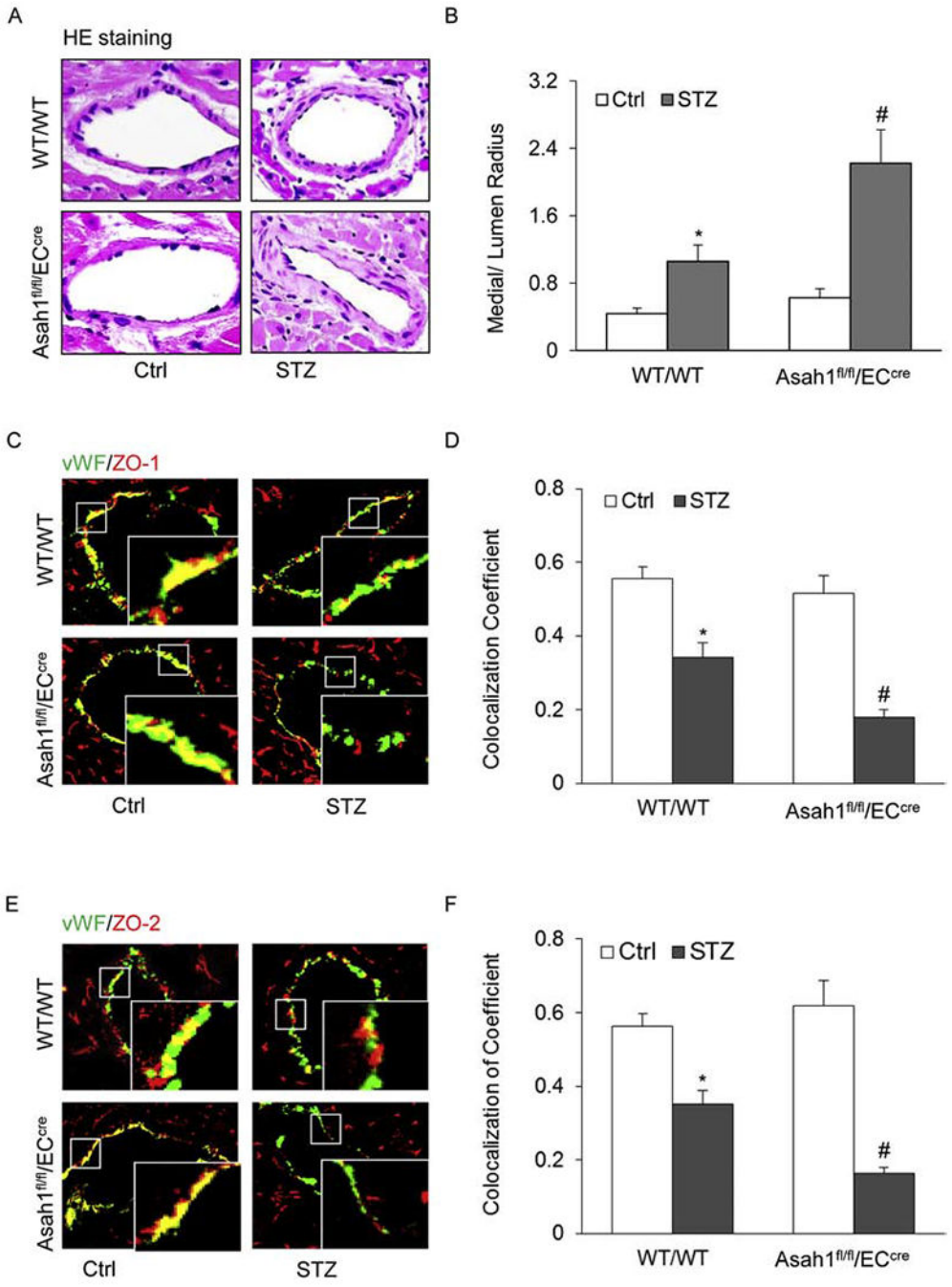

Fig. 2. AC deficiency enhanced mouse coronary arterial thickening and tight junction injury in STZ-treated mice.

A. Representative Hematoxylin and Eosin (HE) staining showing potential medial thickening from the coronary arterial wall of WT/WT and *Asah1*$^{fl/fl}$/EC^{cre} mouse. B. The summarized data showing the measured media/lumen ratio of the coronary arteries from mice with different treatments. C. Representative fluorescent confocal microscopic images displaying the yellow dots or patches showing the colocalization of vWF (green) with ZO-1 (red), a tight junction protein. D. The summarized data showing the change of the colocalization coefficient of vWF with ZO-1. E. Representative fluorescent confocal

microscopic images displaying the yellow dots or patches showing the colocalization of vWF (green) with ZO-2 (red), a tight junction protein. F. The summarized data showing the change of the colocalization coefficient of vWF with ZO-2. Data are expressed as means ± SEM, n=5. * $p<0.05$ vs. WT/WT-Ctrl group; # $p<0.05$ vs. WT/WT-STZ.

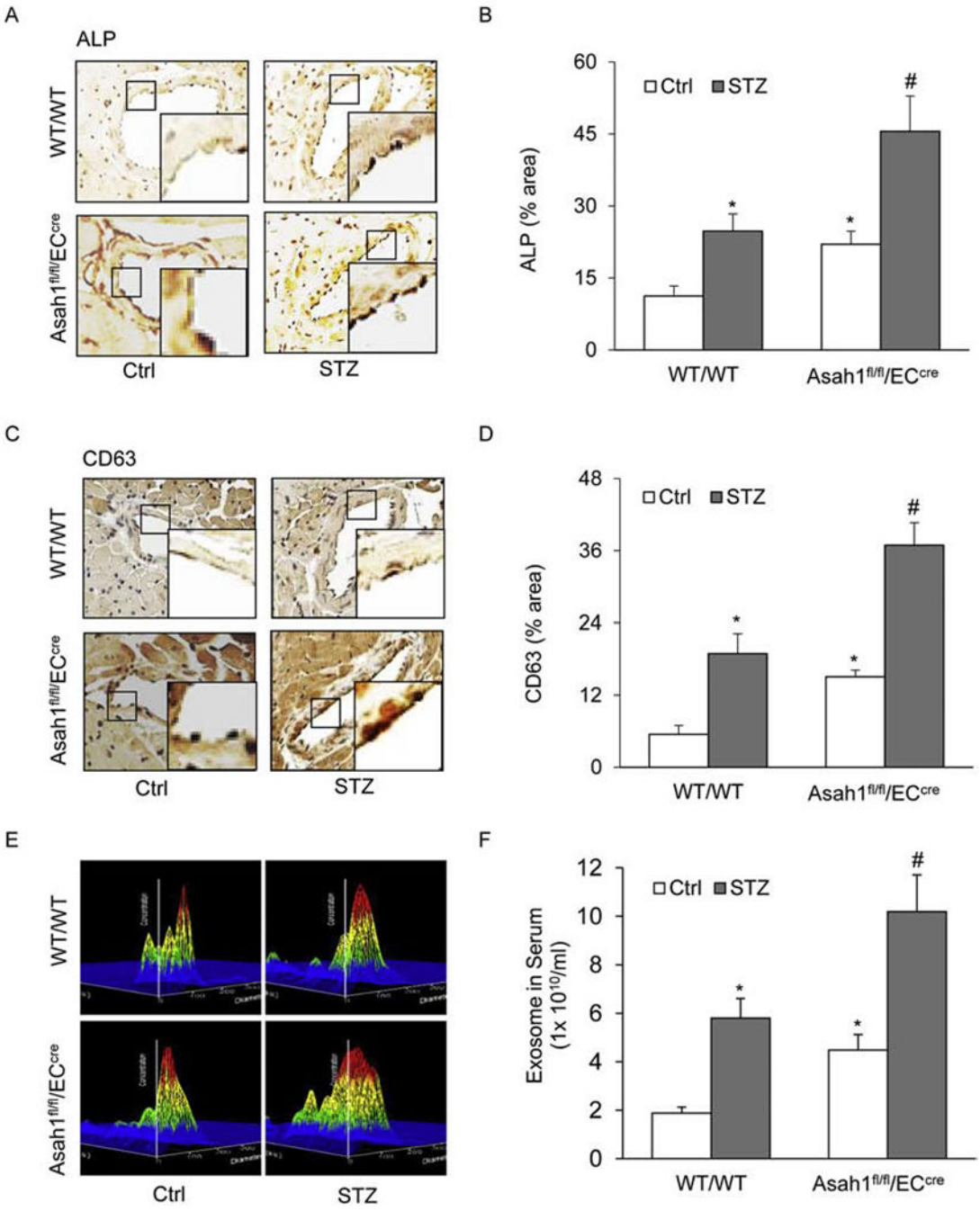

Fig. 3. AC deficiency enhances exosome secretion in the coronary arterial endothelium of STZ-treated mice.

A. Representative microscopic images of tissue slide with IHC staining showing the expression of exosome marker CD63 in the mouse coronary arterial wall. B. The summarized data showing the density of CD63 stained with the anti-CD63 antibody. C. Representative microscopic images of tissue slide with IHC staining showing the expression of exosome marker ALP in the mouse coronary arterial wall. D. The summarized data showing the density of ALP stained with the anti-ALP antibody. E. Representative 3D histograms showing the secretion of exosomes in the mouse serum as measured by

nanoparticle tracking analysis (NTA) using NanoSight NS300 nanoparticle analyzer. F. The summarized data showing the released exosomes in the serum. Data are expressed as means ± SEM, n=5. * $p<0.05$ vs. WT/WT-Ctrl group; # $p<0.05$ vs. WT/WT-STZ.

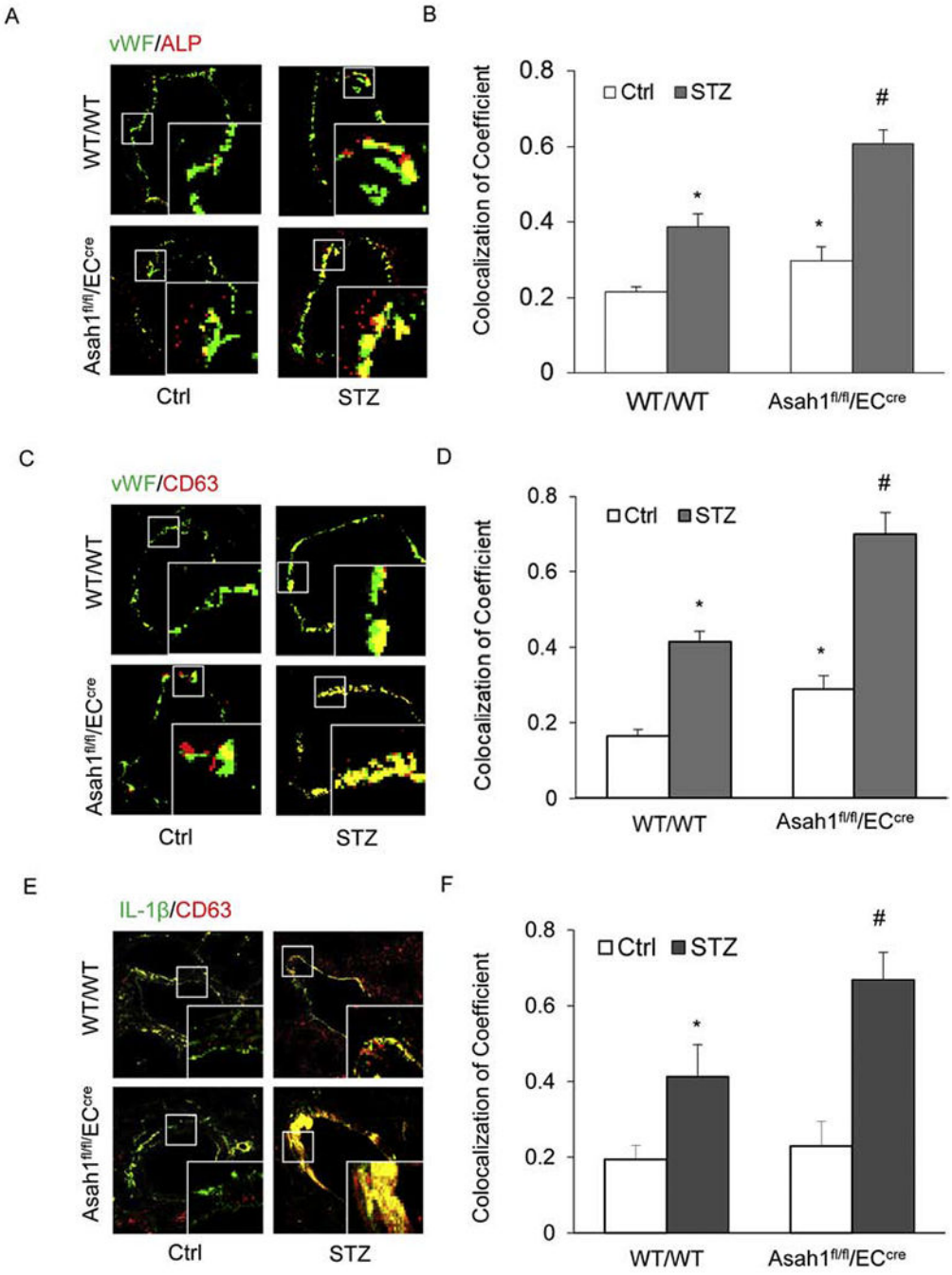

Fig. 4. AC mediates the release of NLRP3 inflammasome products IL-1β.

A. Representative fluorescent confocal microscopic images displaying the yellow dots or patches showing the colocalization of vWF (green) with CD63 (Red). B. The summarized data showing the colocalization coefficient of vWF with CD63. C. Representative fluorescent confocal microscopic images showing the colocalization of vWF (green) with ALP (Red). D. The summarized data showing the colocalization coefficient of vWF with ALP. E. Representative fluorescent confocal microscopic images showing the colocalization of IL-1β (green) with CD63 (Red). F. The summarized data showing the colocalization

coefficient of IL-1β with CD63. Data are expressed as means ± SEM, n=5. * $p<0.05$ vs. WT/WT-Ctrl group; # $p<0.05$ vs. WT/WT-STZ.

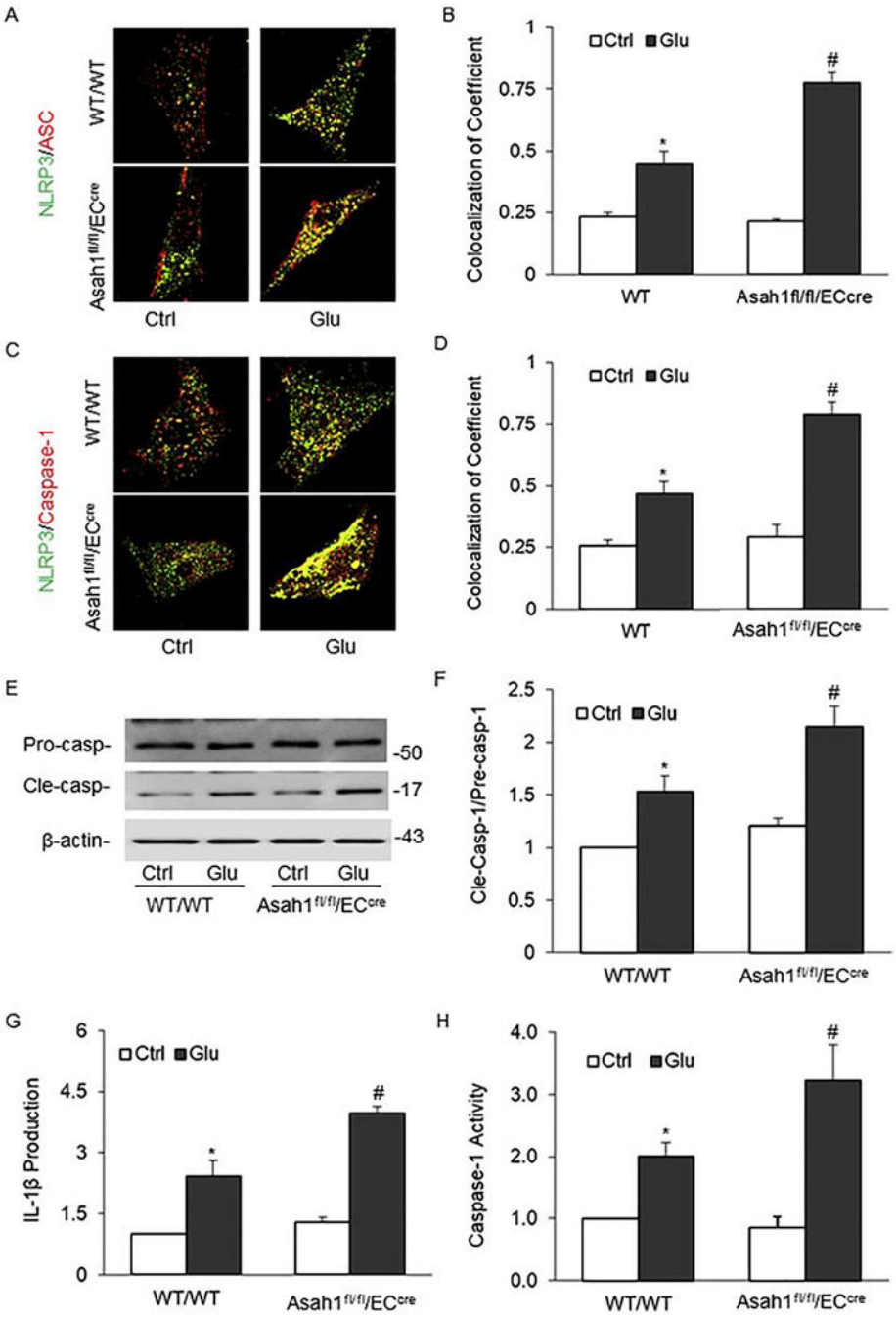

Fig. 5. Effects of AC on the activation and formation of NLRP3 Inflammasome in the primary cultures of coronary arterial endothelial cells (ECs) induced by high glucose.

A. Representative fluorescent confocal microscopic images showing the colocalization of NLRP3 with *ASC.* B. The summarized data showing the colocalization coefficient of NLRP3 vs. *ASC. C.* Representative fluorescent confocal microscopic images showing the colocalization of NLRP3 vs. Caspase-1. D. The summarized data showing the colocalization coefficient of NLRP3 vs. Caspase-1. E. Representative Western blot gel documents showing the expression of procaspase-1 and cleaved caspase-1 induced by high glucose. F. The summarized data showing the ratio of cleaved caspase-1 with procaspase-1 induced by high

glucose. G. The summarized data showing caspase-1 activity (n=5). B. The summarized data showing IL-1β production. Glu: Glucose. Data are expressed as means ± SEM, n=5. * $p<0.05$ vs. WT/WT-Ctrl group; # $p<0.05$ vs. WT/WT-STZ.

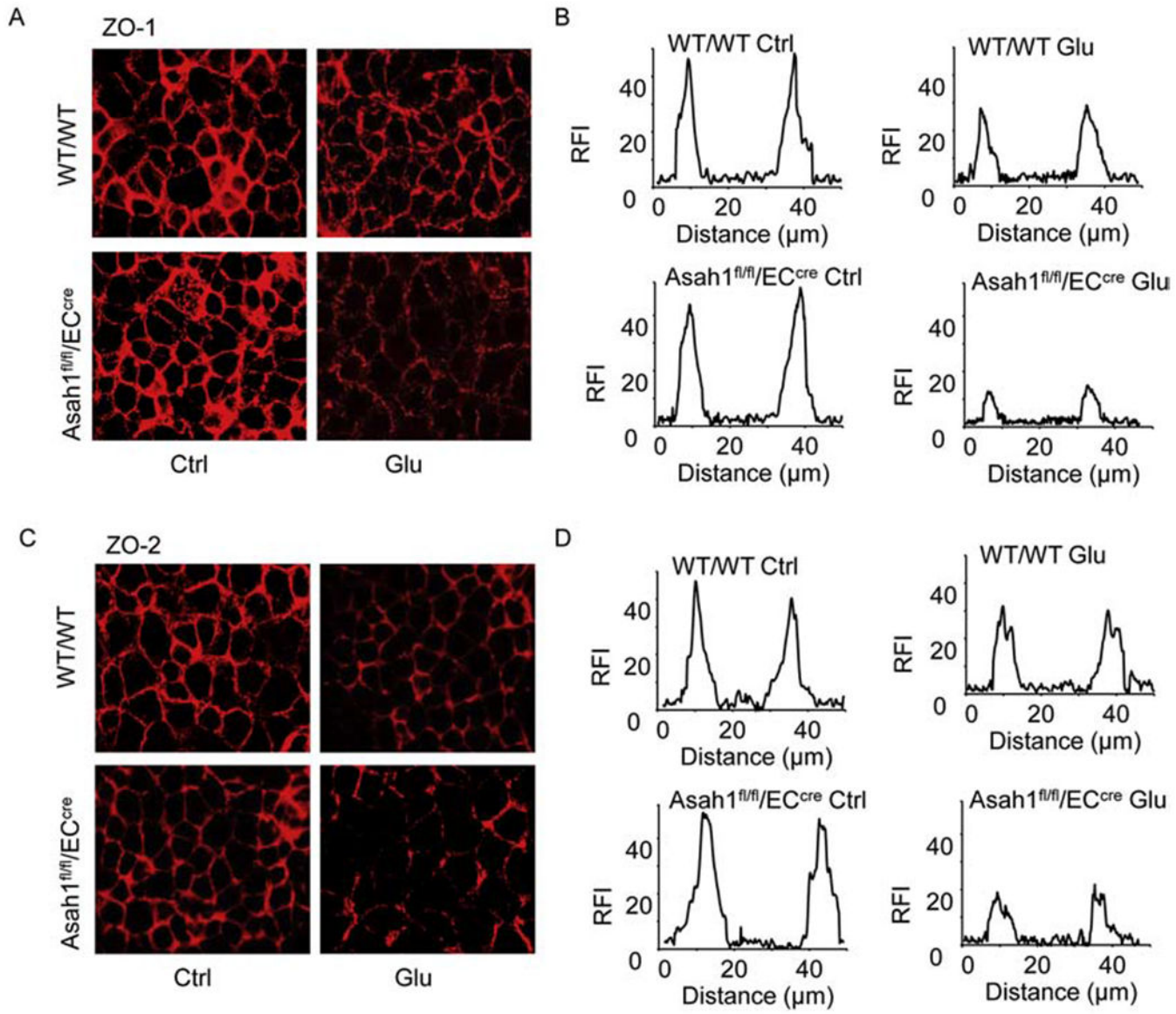

Fig. 6. Effects of AC on the high glucose-induced disruption of tight junction proteins in coronary arterial ECs.

A. Representative fluorescent images showing the cell membrane fluorescence of ZO-1 from at least three independent experiments. B. Tight junctions are represented by histograms of ZO-1 fluorescence intensity (RFI) as indicated by dotted lines across the two cell-cell contacts. C. Representative fluorescent images showing the cell membrane fluorescence of ZO-2 from at least three independent experiments. B. Tight junctions are represented by histograms of ZO-2 fluorescence intensity (RFI) as indicated by dotted lines across the two cell-cell contacts.

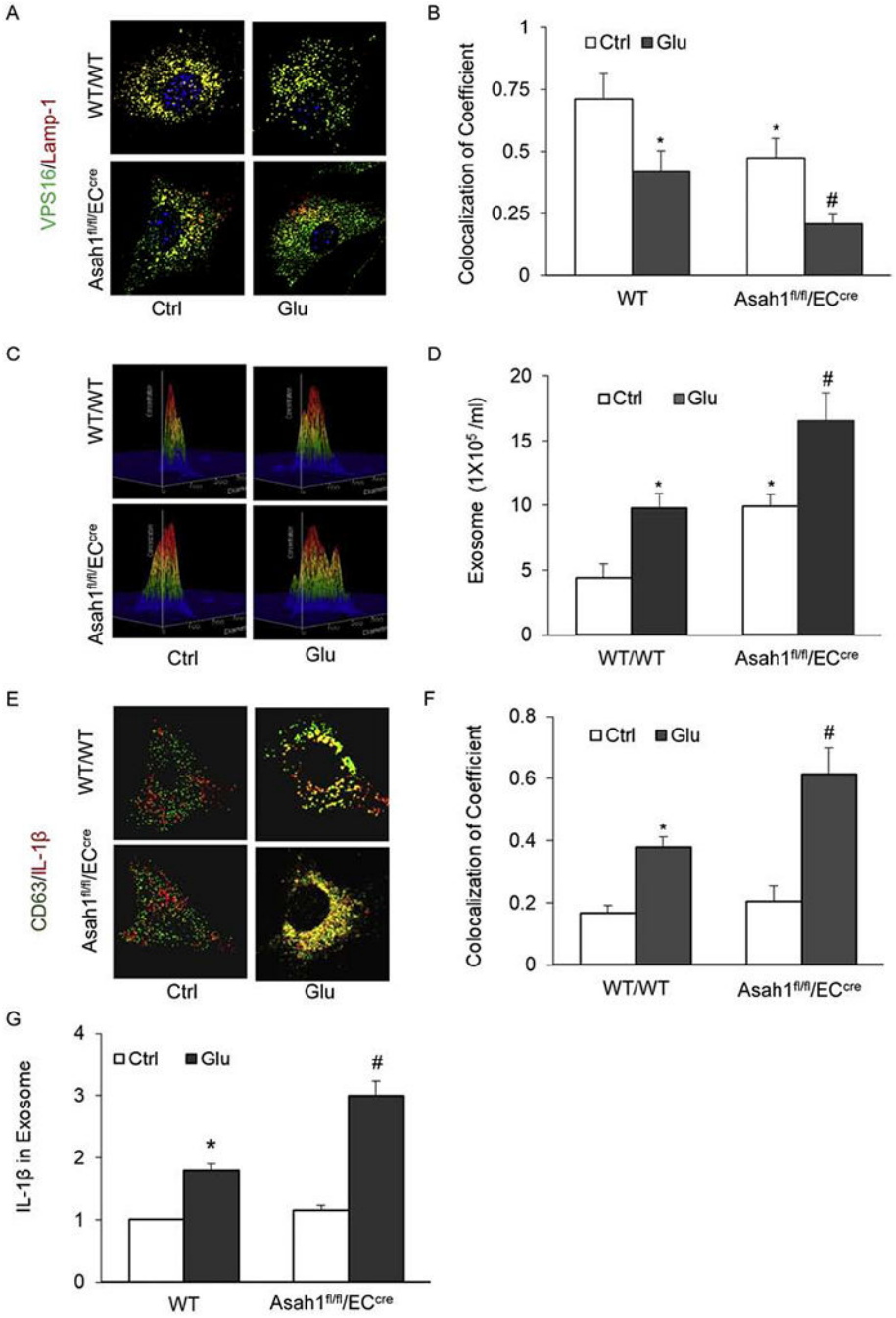

Fig. 7. Effects of AC on high glucose-induced exosome secretion in coronary arterial ECs.

A. Representative fluorescent confocal microscopic images showing the colocalization of VPS 16 (green) with Lamp-1 (Red). B. The summarized data showing the colocalization coefficient of VPS16 (green) with Lamp-1 (Red). C. Representative 3D histograms showing the secretion of exosomes in the cell culture medium as measured by nanoparticle tracking analysis (NTA) using NanoSight NS300 nanoparticle analyzer. D. The summarized data showing the released exosomes in the cell culture medium (50-150 nm). E. Representative fluorescent confocal microscopic images showing the colocalization of CD63 (green) with

IL-1β (red). F. Summarized data showing the colocalization coefficient of CD63 with IL-1β. G. The summarized data showing the released IL-1β in the cell culture medium. Data are expressed as means ± SEM, n=5. * $p<0.05$ vs. WT/WT-Ctrl group; # $p<0.05$ vs. WT/WT-STZ.